Anderson lattice behavior in $Yb_{1-x}Lu_xAl_3$

E. D. Bauer,[1] C. H. Booth,[2] J. M. Lawrence,[3] M. F. Hundley,[1] J. L. Sarrao,[1] J. D. Thompson,[1]
P. S. Riseborough,[4] and T. Ebihara[5]
[1]*Los Alamos National Laboratory, Los Alamos, New Mexico 87545, USA*
[2]*Lawrence Berkeley National Laboratory, Berkeley, California 94720, USA*
[3]*University of California, Irvine, California 92697, USA*
[4]*Temple University, Philadelphia, Pennsylvania 19122, USA*
[5]*Shizuoka University, Shizuoka 422-8529, Japan*
(Received 6 October 2003; published 12 March 2004)

Measurements of magnetic susceptibility $\chi(T)$, specific heat $C(T)$, Hall coefficient $R_H(T)$, and Yb valence $\nu=2+n_f$ [f-occupation number $n_f(T)$ determined from Yb L_{III} x-ray absorption measurements] were carried out on single crystals of $Yb_{1-x}Lu_xAl_3$. The low-temperature anomalies observed in $\chi(T)$ and $C(T)$ corresponding to an energy scale $T_{coh}\sim 40$ K in the intermediate valence, Kondo lattice compound $YbAl_3$ are suppressed by Lu concentrations as small as 5% suggesting these low-T anomalies are extremely sensitive to disorder and, therefore, are a true coherence effect. By comparing the temperature dependence of various physical quantities to the predictions of the Anderson impurity model, the slow crossover behavior observed in $YbAl_3$, in which the data evolve from a low-temperature coherent, Fermi-liquid regime to a high-temperature local moment regime more gradually than predicted by the Anderson impurity model, appears to evolve to fast crossover behavior at $x\sim 0.7$ where the evolution is more rapid than predicted. These two phenomena found in $Yb_{1-x}Lu_xAl_3$, i.e., the low-T anomalies and the slow/fast crossover behavior are discussed in relation to recent theories of the Anderson lattice.

DOI: 10.1103/PhysRevB.69.125102 PACS number(s): 71.27.+a, 71.28.+d, 75.30.Mb, 75.20.Hr

I. INTRODUCTION

Materials with a periodic array of f-electron atoms in a metallic host provide a wealth of phenomena with which to investigate strongly correlated electron physics. A large number of these so-called ''Kondo lattice'' systems are heavy fermion materials which can exhibit magnetically ordered or nonmagnetic ground states, unconventional superconductivity, or non-Fermi-liquid behavior if they reside close to a quantum critical point.[1–3] Still another class of Kondo lattice compounds exhibit intermediate valence (IV) behavior (for a review see Refs. 4–6). These mixed valence materials are often less complex than heavy fermion compounds because the Kondo temperature of the IV materials is usually an order of magnitude larger than the crystalline electric-field (CEF) splitting so CEF effects can be neglected, anisotropy and low dimensionality do not play an important role since most IV compounds are cubic, and most IV materials have nonmagnetic, Fermi-liquid ground states. In addition, the physical properties of such materials are often qualitatively described by the Anderson impurity model (AIM), despite the fact that these are concentrated, stoichiometric systems, and are governed by a single energy scale (Kondo temperature T_K) and, therefore, scale as some function of T/T_K. Thus, the simplicity of these intermediate valence systems provides a unique opportunity to investigate the extension of the AIM to the physics of Kondo lattice compounds described by the Anderson lattice (AL) model.

Generalizing the AIM to a periodic lattice of Kondo impurities has attracted the attention of both theorists and experimentalists alike in recent years. While no complete solution of the AL exists as of yet, a number of theories have been proposed which point to distinct, observable differences between the AL and AIM. ''Protracted (contracted) screening,'' or slow (fast) crossover behavior can occur in the AL, in which the crossover from a coherent, Fermi-liquid ground state at low-temperatures to a high temperature local-moment regime is slower (faster) than predicted by the AIM.[7] In addition, anomalies in the physical properties such as magnetic susceptibility $\chi(T)$ and specific heat $C(T)$ associated with the presence of a second energy scale related to lattice coherence (in addition to the normal Kondo scale) are predicted for the AL.[8–10] Experimentally, the situation is much more complex; some IV materials display slow crossover behavior [e.g., $YbXCu_4$ (X=Mg, Cd)],[11] others exhibit only a low-T anomaly (e.g., $CePd_3$),[12] some show signatures of both types of behavior (e.g., $YbAl_3$),[13] while still other IV compounds are quantitatively well described by the AIM [e.g., $YbXCu_4$ (X=Tl)].[11] A central question is: under what conditions do these signatures of AL behavior occur? Dynamical mean-field calculations[7] of the AL indicate slow crossover behavior can occur when the conduction electron density is small $n_c\ll 1$ (related to Nozières idea of ''Kondo exhaustion''[14]), while fast crossover behavior is found for $n_c\sim 1$. Large-N_J approaches[9,10] to the AL also predict the presence of a second energy scale T_{coh} which is an order of magnitude smaller than the bare Kondo temperature in the limit of small n_c. Recent theoretical work by Burdin *et al.*[10] suggests that the shape of the host density of states (DOS) may be important for the appearance of the second energy scale, which can be either smaller or larger than T_K. In addition, the shape of the DOS may be relevant for either slow or fast crossover behavior.

The IV compound $YbAl_3$ is characterized by a broad maximum at $T_{max}\sim 125$ K in the magnetic susceptibility and also in the specific heat corresponding to a Kondo tempera-

ture $T_K \sim 500$ K.[5,13,15] The electrical resistivity ρ is typical of Kondo lattice compounds and exhibits a decrease in scattering below ~ 100 K due to the formation of Bloch waves and a Fermi-liquid ground state [i.e., $\rho(T) \sim AT^2$] below 40 K.[16] Optical conductivity measurements[17] at 7 K reveal a narrow Drude-like response corresponding to heavy quasiparticle masses ($m^* \sim 25$–$30\ m_e$) and another mid-infrared (IR) peak at ~ 0.15–0.2 eV associated with the formation of a pseudogap, or hybridization gap, as the *f*-electrons hybridize with the conduction electrons. Above 40 K, the Drude peak broadens and the mid-IR peak is suppressed, but below 40 K, the optical spectra do not change appreciably indicating a fully coherent ground state is formed with an energy scale $T_{coh} \sim 40$ K. This interpretation is supported by inelastic neutron scattering experiments[18,19] (INS) which show a narrow peak at ~ 30 meV associated with a hybridization gap that vanishes above 50 K in addition to the broad Lorentzian spectrum centered at $E_0 = 40$ meV corresponding to a Kondo scale $T_K \sim 500$ K. Additional anomalies are found in $\chi(T)$ and $C(T)$ indicating an enhancement of the effective mass in $YbAl_3$ and are associated with a low-temperature energy scale $T_{coh} \sim 40$ K.[13] de Haas–van Alphen experiments[20] show that the effective mass along the $\langle 111 \rangle$ direction in magnetic fields $B = B^* > 40$ T are reduced by a factor of 2 without a significant alteration of the shape of the Fermi surface. The low-T anomaly in $\chi(T)$ is suppressed in a magnetic field $B > 40$ T, of the order $B^* \sim k_B T_{coh}$, indicating that the mass renormalization and suppression of the low-T anomalies below T_{coh} are intimately related. These anomalies are also suppressed in $Yb_{1-x}Lu_xAl_3$ by a Lu concentration $x \sim 0.05$ providing evidence they are very sensitive to disorder and are a true coherence effect.[20]

In this article, we elaborate on our initial report[20] on the physical properties of the $Yb_{1-x}Lu_xAl_3$ system ($0 \leqslant x \leqslant 1$) including magnetic susceptibility, specific heat, Hall coefficient $R_H(T)$, and *f*-occupation number $n_f(T)$ measured by the L_{III} x-ray absorption spectra of Yb. In particular, attention is focused on elucidating the nature of two properties of $YbAl_3$ by means of Lu substitution: (1) the low-T anomalies observed in $\chi(T)$ and $C(T)$, and (2) the slow-crossover behavior found in the parent compound. As briefly noted previously,[20] only small amounts of Lu ($\sim 5\%$) in $YbAl_3$ are needed to completely suppress the extra mass enhancement below T_{coh}. In addition, the physical properties of the $Yb_{1-x}Lu_xAl_3$ system are compared to predictions of the AIM within the noncrossing approximation (NCA). This comparison suggests there is an evolution from the slow crossover behavior observed in $YbAl_3$ to fast crossover behavior at $x \sim 0.7$. It is reasonable to assume that these two experimental results in $Yb_{1-x}Lu_xAl_3$ are related to dilution of the Yb lattice and a connection to existing theories of the AL is made.

II. EXPERIMENTAL DETAILS

Single crystals of $Yb_{1-x}Lu_xAl_3$ were grown in Al flux. The elements were placed in an alumina crucible in the ratio Yb:Lu:Al$=(1-x):x:9$ and sealed in a quartz tube under vacuum. Two different growth cycles were used which yielded high-quality single crystals with typical dimensions of $5 \times 5 \times 5$ mm^3. The materials were heated to 1100 °C and kept there for 2 h. For $x < 0.5$, the temperature was then lowered to 900 °C at a rate 20 °C h^{-1} followed by a slower cooling rate of 4 °C h^{-1} to 650 °C at which point excess Al flux was removed in a centrifuge. For $x \geqslant 0.5$, a single cooling rate from 1100 °C to 650 °C of 4 °C h^{-1} was used.

The magnetic susceptibility measurements were performed in a SQUID magnetometer (Quantum Design) at LANL from 2–300 K in a magnetic field $H = 1$ kOe. High-temperature magnetic susceptibility measurements were performed in an identical SQUID magnetometer at LBNL from 2–800 K in a magnetic field $H = 50$ kOe. In some cases, a small Curie tail (with a Curie constant of the order 10^{-2} cm^3 K/mol) was subtracted from the data. The specific heat was measured from 2–300 K using a thermal relaxation method. The Hall-effect measurements were performed from 2–300 K in $H = 10$ kOe using a linear research LR-700 ac-resistance bridge with an excitation current of 3 mA.

The x-ray absorption near edge spectroscopy (XANES) experiments were carried out at the Yb and Lu L_{III} edges on beam lines 4-1 and 11-2 with a half-tuned Si(220) double-crystal monochromator. The samples were ground, passed through a 30 μm sieve, and mixed with BN powder in appropriate amounts such that the absorption edge step height was approximately unity. A liquid He flow cryostat was used to control the temperature between 20 K and 600 K.

III. THEORETICAL DETAILS

The relevant physical properties were calculated within the AIM using the noncrossing approximation, as described in detail in Ref. 11. These calculations were found to be in good agreement with those of Bickers *et al.*[21] for the case of Ce. A Gaussian DOS centered at the Fermi energy E_F with width W was used for the conduction electron band, i.e., $N(\epsilon) = e^{-\epsilon^2/W^2}/\sqrt{\pi}W$. The *f*-electron/conduction electron hybridization matrix elements were assumed to be independent of $\mathbf{k}$, e.g., $V_{kf} = V$. Neglecting crystalline electric-field effects, a valid assumption for Yb intermediate valence materials, four parameters are needed to calculate the physical quantities using the AIM: (1) the spin-orbit splitting Δ_{SO} (fixed at 1.3 eV based on photoemission experiments);[22] (2) the width of the conduction electron band W [the value $W = 4.33$ eV was chosen to reproduce the electronic specific-heat coefficient of $LuAl_3$ ($\gamma = 3.8$ mJ/mol-K^2) and has been fixed for all Lu concentrations x]; (3) the hybridization matrix element V, and (4) the *f*-level energy E_f relative to the Fermi energy E_F.

The values of V and E_f were determined by fitting the zero-temperature magnetic susceptibility $\chi(0)$ and *f*-occupation number $n_f(0)$, holding W and Δ_{SO} fixed. The Kondo temperature was calculated using the formula

$$T_K = \left(\frac{V^2}{\sqrt{\pi} W |E_f|} \right)^{1/8} \left(\frac{W}{\Delta_{SO}} \right)^{6/8} W\, e^{-\sqrt{\pi} W |E_f| / 8V^2}, \qquad (1)$$

appropriate for Yb, including spin-orbit splitting effects. The temperature dependence of the magnetic susceptibility,

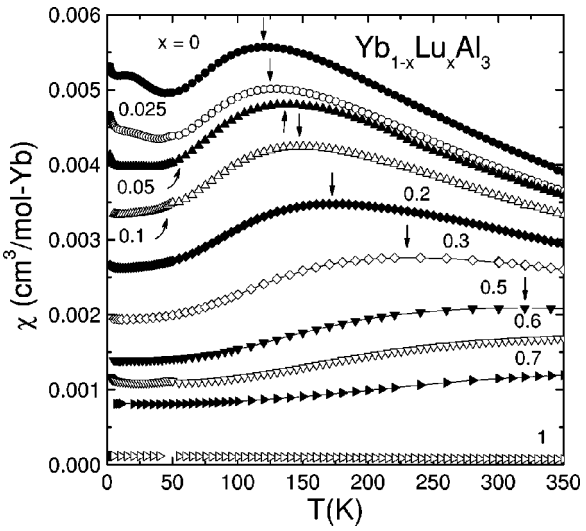

FIG. 1. Magnetic susceptibility $\chi \equiv M/H$ vs temperature T of $Yb_{1-x}Lu_xAl_3$ for various Lu concentrations x. $\chi(T)$ data for $x=0.3$, 0.5, and 0.7 were measured in a magnetic field $H=50$ kOe, for all other concentrations the magnetic field was $H=1$ kOe. The vertical arrows correspond to the temperature (T_{max}) of the maximum in $\chi(T)$.

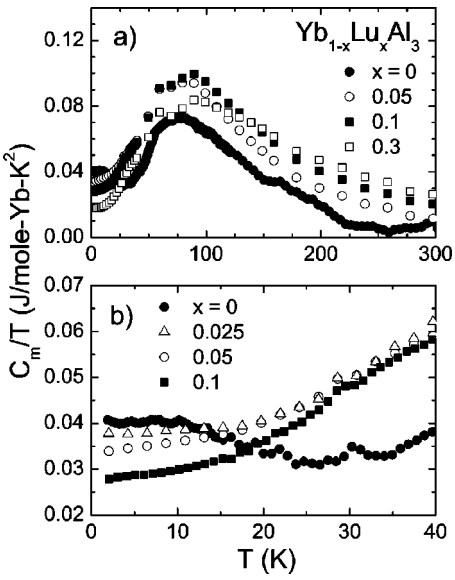

FIG. 2. (a) Magnetic contribution to the specific heat divided by temperature $C_m(T)/T$ of $Yb_{1-x}Lu_xAl_3$ for various Lu concentrations $x \leqslant 0.3$. (b) Expanded view of $C_m(T)/T$ of $Yb_{1-x}Lu_xAl_3$ below 40 K.

f-occupation number, and free energy $F(T)$, along with the energy dependence of the dynamic susceptibility $\chi''(E)$ (at $T=0.01T_K$), were then determined. The electronic specific-heat coefficient γ was obtained by fitting the free energy to the formula $(F(T)=E_0-(\gamma/2)(T/T_K)^2)$ typically between $0.03 \leqslant T/T_K \leqslant 0.07$, with an uncertainty in γ of 5–10%.

IV. RESULTS AND ANALYSIS

A. Magnetic susceptibility

The magnetic susceptibility χ vs temperature T for $Yb_{1-x}Lu_xAl_3$ is shown in Fig. 1. Two main features are visible in the data for low Lu concentrations ($x<0.1$): a broad maximum centered at $T_{max} \sim 125$ K consistent with a Kondo temperature T_K of the order 500 K, and another low-temperature anomaly consistent with a second energy scale of the order $T_{coh} \sim 40$ K. This low-T anomaly is suppressed by $x \sim 0.05$ (as noted previously[20]) and, therefore, is extremely sensitive to disorder. This suggests that the low-T anomaly is associated with lattice coherence. T_{max} shifts to higher temperature with increasing Lu concentrations at a rate $\Delta T_{max}/\Delta x \sim 3.2$ K/at % Lu for $x \leqslant 0.4$. For $x \leqslant 0.5$ the shift of T_{max} increases more rapidly and reaches a value $T_{max}=470$ K at $x=0.7$, above which point no reliable data were obtained. Both the increase in T_{max} and the overall magnitude of χ, which decreases with increasing x, is consistent with an increase of T_K by a factor of 4 or 5 from the value for $x=0$.

B. Specific heat

The magnetic contribution to the specific heat divided by temperature $C_m(T)/T$ of $Yb_{1-x}Lu_xAl_3$, obtained by subtracting the contribution of the nonmagnetic $LuAl_3$ for each data set, is shown in Fig. 2(a) for $x \leqslant 0.3$. The temperature of the maximum observed in $YbAl_3$ at ~ 80 K increases and the peak broadens somewhat with increasing Lu concentration, while the magnitude of C_m/T below 10 K decreases monotonically with increasing x, consistent with an increase in T_K. As shown in Fig. 2(b), the low-T anomaly at $T \sim 15$ K for $x=0$ is rapidly suppressed by Lu substitution; the feature associated with this anomaly is no longer observed for $x \simeq 0.1$, suggesting the low-T anomaly results from lattice coherence. Above $x=0.3$, the difference in specific-heat between $Yb_{1-x}Lu_xAl_3$ and $LuAl_3$ becomes small ($<10\%$ above 100 K) taken together with the decreasing amount of Yb, render the determination of the magnetic contribution to $C(T)$ unreliable. However, the electronic specific heat coefficient is obtained for all x by fitting the data to a sum of electronic and lattice contributions, i.e., $C/T=\gamma+\beta T^2$. Least-squares fits to the data typically below 10 K yield values of γ that decrease monotonically from $\gamma=46$ mJ/mol K^2 for $x=0$ to $\gamma=4$ mJ/mol K^2 for $x=1$ as shown in Fig. 3(a) [the electronic contribution of $LuAl_3$ has been taken into account. i.e., $\gamma_{total}=(1-x)\gamma_{Yb}+x\gamma_{Lu}$], and roughly constant Debye temperatures in the range $\theta_D=380$ K–420 K (results collected in Table I).

C. Hall effect

The temperature dependence of the Hall coefficient $R_H(T)$ is shown in Fig. 4 for various Lu concentrations. At high temperatures above 100 K, R_H exhibits a temperature variation characteristic of scattering from local Yb moments, although a skew-scattering formula does not describe the data well.[13] Large changes in the Hall coefficient are observed below 50 K for $x<0.1$ suggesting significant changes in the Fermi surface topology related to lattice coherence. For $YbAl_3$, R_H becomes negative below 50 K reaching a

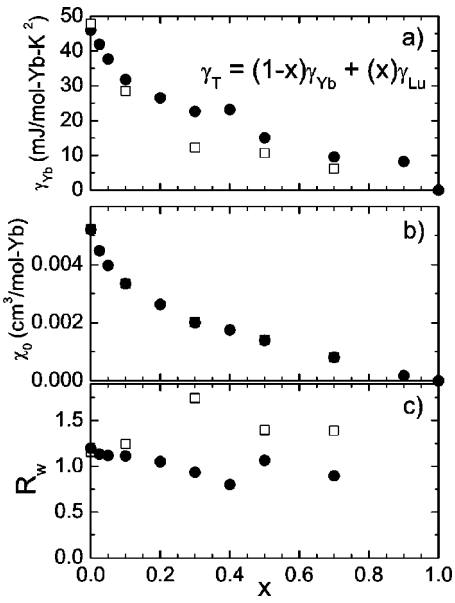

FIG. 3. (a) Yb contribution to the electronic specific-heat coefficient γ_{Yb}, (b) zero-temperature magnetic susceptibility χ_0, and (c) resulting Wilson ratio $\mathcal{R}_W$ vs Lu concentration x for $Yb_{1-x}Lu_xAl_3$. The solid circles are the experimental data and the open squares are the results from the Anderson impurity calculations. (The value of χ_0 in (b) used in the AIM calculations is set equal to the experimental value as discussed in Sec. III.)

value of $R_H = -3\times10^{-10}$ m^3/C at 2 K, while the $x=0.025$ sample exhibits a positive Hall coefficient for $T<50$ K and saturates to $R_H = 2\times10^{-10}$ m^3/C at the lowest temperature. The large variation of R_H for low Lu concentrations are reflected in the value of the Hall coefficient at $T=2$ K, as shown in Fig. 5, in which R_H first exhibits a sharp maximum at $x=0.025$ then decreases nearly monotonically for $x>0.025$. For intermediate Lu concentrations $0.1<x<0.5$, the value of R_H (2 K) is close to zero indicating that both

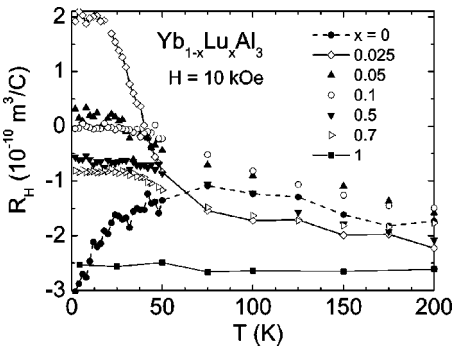

FIG. 4. Temperature variation of the Hall coefficient R_H of $Yb_{1-x}Lu_xAl_3$ for $0\leqslant x\leqslant 1$ measured in a magnetic field $H=10$ kOe.

holelike and electronlike bands contribute to the Hall effect in $Yb_{1-x}Lu_xAl_3$. A monotonic progression to the temperature-independent behavior of $LuAl_3$ (expected for a simple metal) is found for $x\geqslant 0.5$.

D. L_{III} x-ray absorption

The Yb L_{III} x-ray absorption spectrum for $Yb_{0.1}Lu_{0.9}Al_3$ at 150 K is shown in Fig. 6. A weak shoulder is present at 8937 eV arising from divalent Yb absorption in addition to the dominant trivalent Yb edge with a ''white line'' at 8945 eV. The anomaly associated with divalent Yb becomes weaker with increasing temperature; the spectra for other Lu concentrations are comparable and exhibit a similar temperature dependence (not shown). The data were analyzed using the following procedure. In order to account for the disorder inherent in the $Yb_{1-x}Lu_xAl_3$ alloys, which can affect both the amplitude of the white line and the edge line shape, the Lu L_{III}-edge spectrum of a corresponding Lu concentration to the Yb concentration of interest was used as an integral (trivalent) spectrum (i.e., using the Lu L_{III}-edge data of $Yb_{0.9}Lu_{0.1}Al_3$ to model the Yb L_{III}-edge spectrum of

TABLE I. Zero-temperature magnetic susceptibility $\chi(0)$; temperature of maximum in $\chi(T)$, T_{max}; input parameters E_f, V, and calculated Kondo temperature T_K for the AIM calculations [the conduction electron bandwidth $W=4.33$ eV was determined from the value of the electronic specific-heat of $LuAl_3$ ($\gamma=3.8$ mJ/mol K^2) and held fixed for all Lu concentrations x]; and the theoretical and experimental values of the Yb contribution to the electronic specific-heat coefficient γ_{Yb}, Wilson ratio $\mathcal{R}_W$, and inelastic neutron line-shape parameters E_0 and Γ of $Yb_{1-x}Lu_xAl_3$. The inelastic neutron-scattering data are from Ref. 19.

x	$\chi(0)$ (10^{-3}cm^3/mol Yb)	T_{max} (K)	E_f (eV)	V (eV)	T_K (K)	γ_{Yb} (mJ/mol K^2)		$\mathcal{R}_W$		E_0 (meV)		Γ (meV)	
						AIM	expt.	AIM	expt.	AIM	expt.	AIM	expt.
0	5.2	121	−0.58264	0.3425	670	47.8	46	1.16	1.20	43	44	13	24
0.05	4.0	140					37.7		1.12				
0.1	3.3	148	−0.5430	0.3477	1071	28.5	31.8	1.25	1.11	62	~44	28	30
0.2	2.6	177					26.6		1.05				
0.3	2.0	220	−0.9100	0.4735	1642	12.3	22.6	1.74	0.94	105	~44[a]	32	33-35[a]
0.4	1.8	250					23.2		0.80				
0.5	1.4	320	−0.988	0.518	2386	10.7	15.1	1.40	1.06	136	69	66	
0.7	0.8	470	−1.430	0.6715	3967	6.2	9.6	1.39	0.90	97		61	
0.9	0.2						8.3						

[a]Data for $x=0.35$ sample from Ref. 19.

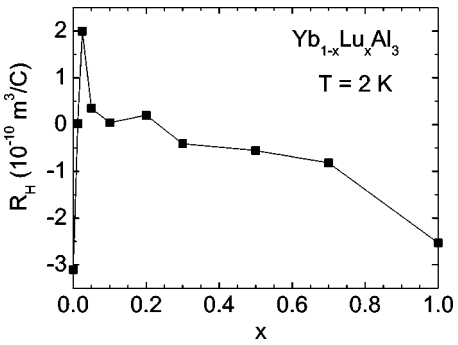

FIG. 5. Hall coefficient R_H at $T=2$ K vs Lu concentration x of $Yb_{1-x}Lu_xAl_3$ for $0\leqslant x\leqslant 1$.

$Yb_{0.1}Lu_{0.9}Al_3$). The Yb-edge data was then fit to a sum of replicas, one representing trivalent absorption with a white line at 8945 eV, and the other spectrum corresponding to divalent absorption with a white line at 8937 eV. A typical fit, along with both the divalent and trivalent contributions, is shown in Fig. 6. The temperature variation of the $4f$ hole occupation number $n_f(T)$, determined from the relative weights of the Yb^{2+} and Yb^{3+} spectra for $Yb_{1-x}Lu_xAl_3$ is shown in Fig. 7(a), along with the ground-state values $n_f(0)$ [Fig. 7(b)]. There is a large decrease in the zero-temperature f-occupation number for $x<0.1$ followed by a smaller, near monotonic decrease for $x\geqslant 0.1$.

E. Anderson impurity calculations

The main results of the Anderson impurity calculations for $Yb_{1-x}Lu_xAl_3$ along with the experimental $\chi(T)$ and $n_f(T)$ data are shown in Figs. 8 and 9, respectively. The data for $x\leqslant 0.1$ crossover from a coherent, Fermi-liquid ground state to high-temperature local-moment behavior [i.e., Curie-Weiss behavior and a saturated $n_f(T)$] more slowly than predicted by the AIM calculations (referred to as ''slow crossover''). There is somewhat reasonable agreement between the data and the theoretical predictions for $x=0.3$ and 0.5. For $x=0.7$, both $\chi(T)$ and $n_f(T)$ appear to exhibit ''fast crossover'' behavior, i.e., the data approach a high-

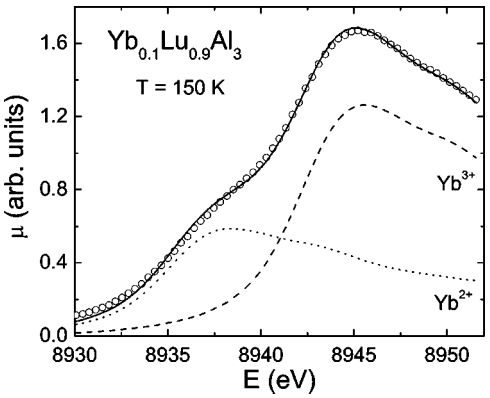

FIG. 6. Yb $L_{\rm III}$ x-ray absorptance μ vs photon energy E at 150 K of $Yb_{0.1}Lu_{0.9}Al_3$ along with an example of a fit (solid line) of the data to the divalent (dotted line) and trivalent (dashed line) integral-valence replicas as discussed in the text in Sec. IV D.

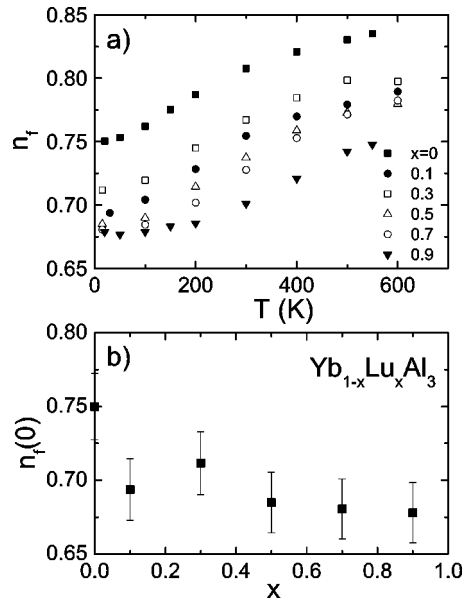

FIG. 7. (a) f-occupation number $n_f(T)$ of $Yb_{1-x}Lu_xAl_3$ for $0\leqslant x\leqslant 0.9$ determined from fits of the $L_{\rm III}$ absorption edge data as discussed in Sec. IV D. (b) Zero-temperature f-occupation number $n_f(0)$ of $Yb_{1-x}Lu_xAl_3$.

temperature local-moment regime more rapidly than the AIM theory predicts. The values of E_f and V used to reproduce the experimentally determined $\chi(0)$ and $n_f(0)$ along with the resulting Kondo temperature [Eq. (1)] are shown in Fig. 10. The Kondo temperature is a sensitive function of the ratio of V^2/E_f and the increase of T_K (inferred from magnetic susceptibility and specific heat) could either be due to a greater

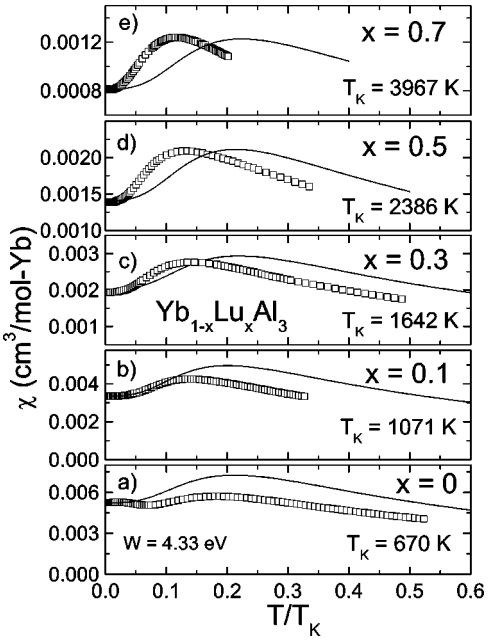

FIG. 8. Magnetic susceptibility χ vs scaled temperature T/T_K for $Yb_{1-x}Lu_xAl_3$. The open squares are the data and the solid lines are Anderson impurity calculations using the parameters listed in Table I.

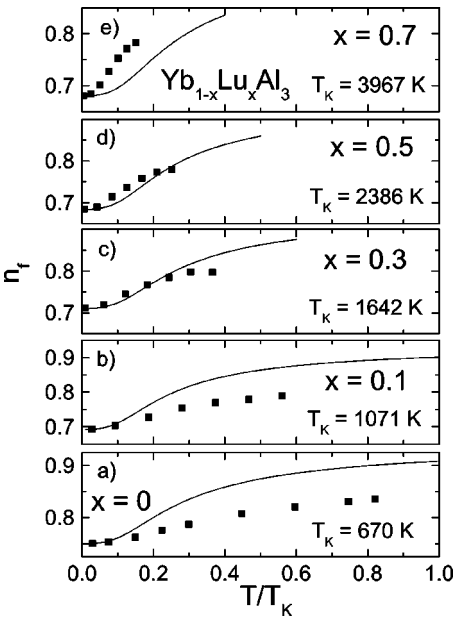

FIG. 9. (a) $4f$ occupation number $n_f(T)$ vs scaled temperature T/T_K for $Yb_{1-x}Lu_xAl_3$. The filled squares are the data and the solid lines are Anderson impurity calculations using the parameters listed in Table I.

amount of hybridization as x increases or caused by a shift of the Yb f level closer to the Fermi level, or a combination of both. A variation of the host DOS $N(E_F)$ may also play a role. The large changes in T_K are presumably not due to a chemical pressure effect since the lattice parameter of $YbAl_3$ ($a=4.203$ Å) and $LuAl_3$ ($a=4.190$ Å) differ by only $\sim 0.3\%$. The f-occupation number n_f also depends on V, E_f, and $N(E_F)$ which is given by the formula (valid in the Kondo limit):[21]

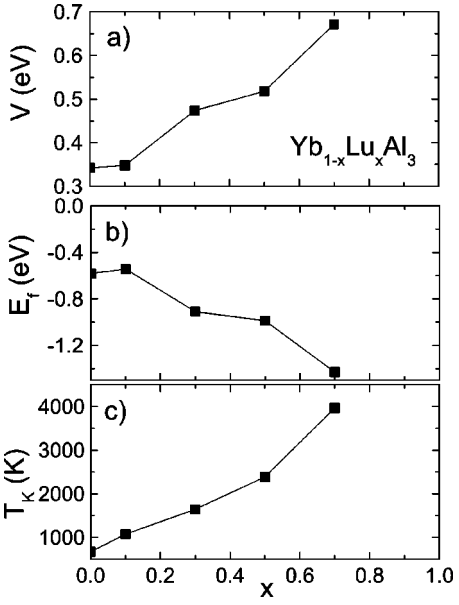

FIG. 10. Anderson impurity calculation parameters (a) hybridization matrix element V, (b) f-level energy E_f, and (c) Kondo temperature T_K vs Lu concentration x for $Yb_{1-x}Lu_xAl_3$.

$$n_f(0)=\frac{1}{1+\dfrac{N_J V^2 N(E_F)}{\pi T_K}} \tag{2}$$

where $N_J=2J+1$ is the orbital degeneracy ($=8$ for Yb). In order for there to be a relatively small decrease in $n_f(0)$ (Fig. 7) concomitant with a large increase in T_K (by a factor of 4 or more) in $Yb_{1-x}Lu_xAl_3$ as x increases, a combination of an increase in V and a decrease in E_f (relative to the Fermi level) must occur (Fig. 10). [$N(E_F)$ is assumed to be constant and is fixed to the value associated with the electronic specific-heat coefficient $\gamma=3.8$ mJ/mol K^2 of $LuAl_3$ in these calculations.] While the values of E_f and V that are obtained by applying the AIM to $\chi(0)$ and $n_f(0)$ are unique, they may not be valid for the actual compound. Since a central message of this paper is that the AIM does not quantitatively describe the behavior of these compounds, the relatively large increase in magnitude of E_f from -0.58 eV at $x=0$ to -1.43 eV at $x=0.7$ and the increase in V should be regarded as a result of a parameterization of the low-T properties of $Yb_{1-x}Lu_xAl_3$ and most likely does not correspond to the true electronic structure of Yb in this system.

A comparison between the data and NCA calculations for the Wilson ratio $\mathcal{R}_W \equiv (\pi^2 k_B^2/\mu_{eff}^2)(\chi(0)/\gamma)$ in addition to $\chi(0)$ and the Yb contribution to the electronic specific-heat γ_{Yb} are displayed in Fig. 3. There is reasonable agreement between the data and theoretical AIM predictions for the Wilson ratio, which is roughly consistent with the expected value $\mathcal{R}_W=(\pi^2 k_B^2 \chi(0)/\mu_{eff}^2\gamma)[1+1/2J]=8/7$,[23] considering the uncertainties in calculating γ. In addition, uncertainties in determining $\chi(0)$ due to Curie-tail contributions may also account for discrepancies between the experimental and theoretical values.

The predicted dynamic susceptibility $\chi''(E)$ (assumed to follow a Lorentzian power spectrum) and associated width Γ (not shown) are also compared to inelastic neutron scattering measurements on $Yb_{1-x}Lu_xAl_3$;[19] in general, agreement between the two results is reasonable for low Lu concentrations ($x \leqslant 0.1$), where the experimental spectra can be modelled by a narrow Lorentzian peak at ~ 34 meV corresponding to transitions across a hybridization gap and another broad Lorentzian typical of mixed-valence systems. For higher Lu concentrations, the INS spectra reveal one broad peak centered at $E_0=69$ meV for $x=0.5$, whereas the NCA calculations predict a peak at $E_0=136$ meV. The origin of this discrepancy in part may be from differences between the polycrystalline samples used for the INS measurements which have substantially different values of $\chi(0)(x \geqslant 0.35)$ than the single-crystal samples upon which the AIM calculations were based. The parameters used in the Anderson impurity calculations, the predicted zero-temperature properties, and Wilson ratio $\mathcal{R}_W$, are collected in Table I.

V. DISCUSSION

Two main results from the experimental data and AIM calculations of $Yb_{1-x}Lu_xAl_3$ provide strong evidence for AL behavior in this system: the rapid suppression of the low-T

anomaly in $\chi(T)$ and $C(T)$ at $\sim$40 K for $x<0.1$ related to the Kondo lattice coherence (the large changes in the Hall coefficient also support this hypothesis) and the apparent evolution from slow crossover ($x\leqslant 0.1$) to fast crossover ($x\sim 0.7$) behavior. Various AL theories, valid both in the Kondo limit[8–10] and in the mixed-valence regime,[13] predict a lattice coherence energy scale an order of magnitude smaller than the Kondo temperature, i.e., $T_{coh}\sim T_K/10$, in rough agreement with $YbAl_3$. In $YbAl_3$, large magnetic fields $B^*>40$ T along the $\langle 111\rangle$ direction reduce the effective mass ($m^*\sim 15$–$20\ m_e$) by a factor of two.[20] In this high-field regime, the $\chi(T)$ anomaly at $\sim$40 K is suppressed and the magnetic susceptibility resembles that of a typical mixed-valence system. This evolution from AL behavior to Anderson impurity behavior occurs in magnetic fields of the order of $B^*\sim k_BT_{coh}/gJ\mu_B$, much smaller than the Kondo field $B_K=k_BT_K/gJ\mu_B\sim 250$ T associated with polarization of the $4f$ level, suggests that magnetic fields renormalize the quasiparticle states. Lu substitution in $YbAl_3$ gives rise to similar behavior, although it appears that the addition of Lu produces large changes in the Fermi surface, while magnetic fields do not significantly alter the shape of the Fermi surface. One of the striking results obtained from this investigation of the $Yb_{1-x}Lu_xAl_3$ system is the large variation in the Hall coefficient in the coherence region ($x\leqslant 0.1$). The large decrease in the Hall coefficient below 50 K in $YbAl_3$ is presumably associated with the Yb lattice coherence as the quasiparticle bands become renormalized. The $x=0.025$ sample also exhibits a large temperature dependence of R_H below 50 K (accompanied by a change in sign) (Fig. 4), implying lattice coherence still persists at this Lu concentration. For $x>0.025$, the Hall coefficient no longer shows such extreme coherence effects and eventually becomes similar to the temperature-independent behavior of $LuAl_3$. A possible explanation for the change in sign and the effect of coherence in the $x=0.025$ sample is proposed on the basis of the band structure of $YbAl_3$.[16] From investigations on the effects of impurities (Kondo holes) in a number of intermediate valence/heavy fermion systems, it is widely believed that disruption of lattice coherence affects the bands with the heaviest effective masses to a greater degree than bands with lighter masses. In the case of $YbAl_3$, the heaviest electron and hole branches are the β and ϵ bands, respectively; de Haas–van Alphen measurements[16] yield effective masses of $m^*\sim 27\ m_e(\beta)$ and $m^*\sim 18\ m_e(\epsilon)$. Lu substitution first disrupts the β orbit leading to hole-like (coherent) conduction for $x\sim 0.025$ which is reflected in the change in sign of R_H. The mobility of the ϵ band is rapidly suppressed upon further Lu substitution ($x\sim 0.05$). For $x>0.1$, the numerous lighter mass bands (α, γ, δ, etc.) are affected, but alter the Hall coefficient to a lesser extent than the heaviest mass bands.

Experimental evidence suggests that the temperature dependence of the physical properties of Kondo lattice compounds, such as $YbXCu_4$ ($X=$Cd, Tl) and $YbAl_3$, are substantially different than predicted by the AIM. For instance, $YbMgCu_4$ and $YbZnCu_4$ exhibit slow crossover behavior, where $\chi(T)$, $C(T)$, and $n_f(T)$ approach a high-T, local-moment regime more gradually than expected from AIM calculations.[11] A correlation was found between the carrier concentration and the slow crossover behavior in the $YbXCu_4$ system; the compounds with $n_c<1\ e^-$/atom (e.g., $YbCdCu_4$) displayed slow crossover behavior while the AIM calculations were in quantitative agreement with those compounds with $n_c>1\ e^-$/atom (e.g., $YbAgCu_4$). A similar correlation also exists in $YbAl_3$ in which slow crossover is found in various physical properties, and Hall-effect measurements on $LuAl_3$ imply a carrier concentration $n_c\sim 0.5\ e^-$/atom.[13] One of the central results of the analysis of the current investigation of $Yb_{1-x}Lu_xAl_3$ is the apparent evolution from slow crossover ($x\leqslant 0.1$) to fast crossover behavior ($x\sim 0.7$). While a quantum Monte Carlo investigation of the AL suggests that fast crossover behavior can occur when the carrier concentration is large ($n_c\sim 1$),[7] it is not clear whether this model can provide an explanation for the fast crossover behavior observed in $Yb_{1-x}Lu_xAl_3$ as it is unlikely that the Lu-rich alloys ($x\sim 0.7$) are good metals where $LuAl_3$ is not one. In addition, the role of disorder has not been taken into account in comparing the AIM calculations to the experimental $Yb_{1-x}Lu_xAl_3$ data.

An alternative explanation for the evolution from slow to fast crossover behavior in $Yb_{1-x}Lu_xAl_3$ is provided by a recent theoretical study[10] of the AL which shows that the various energy scales (T_{coh}, etc.) and the slow/fast crossover behavior depend strongly on the host DOS near the Fermi level. In particular, when the Fermi level is close to a maximum in the DOS, the coherence scale is found to be much smaller than the bare Kondo temperature, i.e., the magnetic susceptibility and specific heat are enhanced over the AIM result, and the system displays slow crossover behavior. On the other hand, when the DOS exhibits a minimum near E_F, $T_K\ll T_{coh}$, resulting in both a reduction of $\chi(T)$ and $C(T)$ in comparison to the AIM and also to fast crossover behavior. An intuitive argument for the latter case is provided by Burdin and coworkers.[10] When the Kondo screening cloud begins to develop around the local moments at $T\sim T_K$, only a few states in the vicinity of E_F contribute to the screening process. However, the T_{coh} energy scale is identified with the Fermi-liquid temperature (i.e., associated with the $T=0$ K properties) and is related to the inverse of the large renormalized quasiparticle DOS. This T_{coh} energy scale therefore samples a larger DOS in the case where E_F is located near a minimum in the DOS and hence, $T_K\ll T_{coh}$. Thus, if the shape of the host DOS changed from a local maximum near the Fermi level for low Lu concentrations ($x\leqslant 0.1$) to a local minimum in the vicinity of E_F for high Lu concentrations ($x\sim 0.7$) in $Yb_{1-x}Lu_xAl_3$, an evolution from slow crossover to fast crossover behavior may result, consistent with the theoretical predictions. One possible way this change in the host DOS could come about based on the increase in the Kondo temperature in the $Yb_{1-x}Lu_xAl_3$ system is that a shift in E_F from a maximum to a minimum in the DOS occurs as mixed-valent Yb ($\nu\sim 2.75$) is replaced by trivalent Lu. Band structure calculations of $Yb_{1-x}Lu_xAl_3$ would be helpful in determining if this scenario is correct or not.

Disorder has a profound effect on f-electron systems in the vicinity of a quantum critical point,[2,3,24] but the effect of

disorder on stoichiometric intermediate valence systems in the context of the AL has not been addressed. At present, it cannot be ruled out that the fast crossover observed for large x is a consequence of such disorder. A related issue is when (i.e., at what concentration x) the impurity model should be valid. It is reasonable that the $Yb_{1-x}Lu_xAl_3$ system is still in the AL regime at $x \sim 0.7$ since fast crossover behavior is observed at that Lu concentration, i.e., the data cannot be quantitatively described by the AIM; an estimate in support of this possibility is that the percolation threshold for a cubic lattice in three dimensions is $p = 20\%$.[25] While is expected that $Yb_{1-x}Lu_xAl_3$ will eventually follow the AIM at higher Lu concentrations, experimental evidence for single impurity behavior for $x \geqslant 0.9$ is not conclusive due the large Kondo temperatures, and hence, a very weak temperature dependence and small magnitude of $\chi(T)$ observed in these samples.

VI. CONCLUSIONS

The physical properties of single crystals of $Yb_{1-x}Lu_xAl_3$ have been investigated. The low-T anomalies observed in the parent compound $YbAl_3$ corresponding to an energy scale $T_{coh} \sim 40$ K are extremely sensitive to disorder (Lu substitution) and, thus, are related to lattice coherence. Comparison of the $Yb_{1-x}Lu_xAl_3$ data to the predictions of the AIM suggest there is an evolution from slow crossover behavior ($x \leqslant 0.1$) to fast crossover behavior ($x \sim 0.7$). Recent theoretical work by Burdin *et al.*[10] show that the presence of the coherence energy scale and the slow/fast crossover behavior depend sensitively on the shape of the host DOS near the Fermi level which may be relevant to $Yb_{1-x}Lu_xAl_3$.

ACKNOWLEDGMENTS

Work at Los Alamos was performed under the auspices of the DOE. Work by J. M. L. was supported by the DOE Grant No. DE-FG03-03ER46036. Work at Lawrence Berkeley National Laboratory was supported by the Director, Office of Science, Office of Basic Energy Sciences, of the U.S. Department of Energy under Contract No. DE-AC03-76SF00098. Portions of this research were carried out at the Stanford Synchrotron Radiation Laboratory, a national user facility operated by Stanford University on behalf of the U.S. Department of Energy, Office of Basic Energy Sciences.

[1] A. C. Hewson, *The Kondo Problem to Heavy Fermions* (Cambridge University Press, Cambridge, 1993).
[2] See various articles in Proceedings of the Institute for Theoretical Physics Conference on Non-Fermi Liquid Behavior in Metals, Santa Barbara, 1996, edited by P. Coleman, M.B. Maple, and A.J. Millis, J. Phys.: Condens. Matter **8**, 9675 (1996).
[3] G.R. Stewart, Rev. Mod. Phys. **73**, 797 (2001).
[4] See, for example, *Valence Instabilities and Related Narrow-Band Phenomena*, edited by R. D. Parks (Plenum Press, New York, 1977).
[5] J.M. Lawrence, P.S. Riseborough, and R.D. Parks, Rep. Prog. Phys. **44**, 3 (1981).
[6] See, for example, *Valence Fluctuations in Solids*, edited by L. M. Falicov, W. Hanke, and M. B. Maple (Institute for Theoretical Physics, Santa Barbara, CA, 1981).
[7] A.N. Tahvildar-Zadeh, M. Jarrell, and J.R. Freericks, Phys. Rev. B **55**, 3332(R) (1996); Phys. Rev. Lett. **80**, 5168 (1998).
[8] Y. Ono, T. Matsuura, and Y. Kuroda, J. Phys. Soc. Jpn. **60**, 3475 (1991).
[9] S. Burdin, A. Georges, and D.R. Grempel, Phys. Rev. Lett. **85**, 1048 (2000).
[10] S. Burdin and V. Zlatić, cond-mat/0212222 (unpublished).
[11] J.M. Lawrence, P.S. Riseborough, C.H. Booth, J.L. Sarrao, J.D. Thompson, and R. Osborn, Phys. Rev. B **63**, 054427 (2001).
[12] J.R. Thompson, S.T. Sekula, C.-K. Loong, and C. Stassis, J. Appl. Phys. **53**, 7893 (1982).
[13] A.L. Cornelius, J.M. Lawrence, T. Ebihara, P.S. Riseborough, C.H. Booth, M.F. Hundley, P.G. Pagliuso, J.L. Sarrao, J.D. Thompson, M.H. Jung, A.H. Lacerda, and G.H. Kwei, Phys. Rev. Lett. **88**, 117201 (2002).
[14] P. Nozières, Ann. Phys. (Paris) **10**, 19 (1998); Eur. Phys. J. B **6**, 447 (1998).
[15] E.E. Havinga, K.H.J. Buschow, and H.J. van Daal, Solid State Commun. **13**, 621 (1973).
[16] T. Ebihara, Y. Inada, M. Murakawa, S. Uji, C. Terakura, T. Terashima, E. Yamamoto, Y. Haga, Y. Onuki, and H. Harima, J. Phys. Soc. Jpn. **69**, 895 (2000).
[17] H. Okamura, T. Ebihara, and T. Nanba, Acta Phys. Pol. B **34**, 1075 (2003).
[18] A.P. Murani, Phys. Rev. Lett. **54**, 1444 (1985).
[19] R. Osborn, E. Goremychkin, I.L. Sashin, and A.P. Murani, J. Appl. Phys. **85**, 5344 (1999).
[20] T. Ebihara, E.D. Bauer, A.L. Cornelius, J.M. Lawrence, N. Harrison, J.D. Thompson, J.L. Sarrao, M.F. Hundley, and S. Uji, Phys. Rev. Lett. **90**, 166404 (2003).
[21] N.E. Bickers, D.L. Cox, and J.W. Wilkins, Phys. Rev. B **36**, 2036 (1987).
[22] J.J. Joyce, A.J. Arko, J.L. Sarrao, K.S. Graham, Z. Fisk, and P.S. Riseborough, Philos. Mag. B **99**, 1 (1999).
[23] D.M. Newns, A.C. Hewson, J.W. Rasul, and N. Read, J. Appl. Phys. **53**, 7877 (1982).
[24] M.B. Maple, C.L. Seaman, D.A. Gajewski, Y. Dalichaouch, V.B. Barbetta, M.C. de Andrade, H.A. Mook, H.G. Lukefahr, O.O. Bernal, and D.E. MacLaughlin, J. Low Temp. Phys. **95**, 225 (1994).
[25] D. Stauffer, *Introduction to Percolation Theory* (Taylor & Francis, London, 1985).